Quantitative investigation of the Zeeman and Paschen-Back effects of the hyperfine structure during the rubidium $5\,^2S_{1/2} \rightarrow 5\,^2D_{5/2}$ two-photon transition

Masashi Abe,* Ryohei Itoyama, Yuta Komiyama, Takuma Ito, Taro Mashimo, and Satoshi Tojo
Department of Physics, Faculty of Science and Engineering, Chuo University, Kasuga, Bunkyo-ku, Tokyo 112-8551, Japan

(Received 27 August 2018; published 28 May 2019)

We precisely investigate the Zeeman and Paschen-Back effects of the hyperfine structure during the rubidium $5\,^2S_{1/2} \rightarrow 5\,^2D_{5/2}$ two-photon transition. Owing to the high sensitivity of the D state of atoms to a magnetic field, the splittings of the spectra of the D state are sufficiently large in a weak magnetic field of $<$10 G. We experimentally observe how in the hyperfine coupling in the $5\,^2D_{5/2}$ state is disrupted even in weak magnetic fields around 10 G and the energy levels are arranged according to their total angular momentum J and nuclear spin I. The transient of the spectra known as the Paschen-Back effect is observed even in a weak magnetic field with an order of magnitude of several tens of gauss. The results of theoretical calculations for energy shifts and transition intensities under a magnetic field are in quantitative agreement with the experimental results.

DOI: 10.1103/PhysRevA.99.053420

I. INTRODUCTION

Two-photon transitions are powerful tools for both photonic research in quantum optics and atomic spectroscopy [1,2]. When using thermal atomic vapor, two-photon spectroscopy has the advantage of obtaining precise measurements of nonlinear phenomena such as quantum interferences. Although linear transition probability is proportional to only the laser intensity (square of the magnitude of an electric field), a two-photon excited transition is advantageous for local field measurements with focused beams because the transition probability is proportional to the square of the intensity [3]. Precise spectroscopy using Doppler-free two-photon transitions has been considered for the investigation of the S and D states of alkali-metal atoms, since the resolution of linear spectroscopy is limited by Doppler broadening to a few hundred MHz to 1 GHz at room temperature with visible light [3–6]. Additionally, the Doppler-free two-photon spectra are simpler compared to saturated absorption spectra because crossover lines are not present in the former.

It is well known that, in an external magnetic field, the energy levels of atoms split into $2F + 1$ magnetic sublevels whose energies are shifted, where F is the total angular momentum including the nuclear spin. Additionally, the atomic transition probabilities are changed by the external magnetic field [7]. Alkali-metal atoms are widely used for investigating optical and magneto-optical processes in atomic vapors as well as for cooling of atoms and Bose-Einstein condensates [8–10]. Therefore, detailed knowledge of the behavior of their atomic levels in the presence of a magnetic field is of high interest. In particular, many quantum operations have been performed on the S or P states in a one-photon process with cold atoms. On the other hand, there have been few cases involving other levels, for example, the $5D$ state with a two-photon transition in rubidium (Rb) atoms. For example, although the Faraday effect, which arises due to a magnetic field producing circular birefringence in the medium, plays an important role in quantum memory based on off-resonant magneto-optical interaction between light and atoms [11], it has been studied for the S or P states [12]. Because the D state is more sensitive to the magnetic field, it is easy to observe the Faraday effect and realize spin orientation. It is indispensable to evaluate the mixed wave functions of these levels in order to reveal the Faraday effect of the D state.

The Zeeman and Paschen-Back effects have been studied for investigating nonlinear and transient effects in the presence of a magnetic field [13–15]. In Na atoms, the $3S \rightarrow 4D$ two-photon transition was investigated by applying magnetic fields of 170 [13,16] and 300 G [15]. In Rb atoms, the D_2 line was also investigated by applying a magnetic field of 80 G [17]. However, in view of the splitting coefficient of the P state of alkali-metal atoms, the transitions are unresolved in magnetic fields of several tens of gauss; i.e., it is difficult to investigate the magnetic field effect in $S \rightarrow P$ transitions owing to their broad linewidths. Recently, the Paschen-Back effect, which disrupts the hyperfine coupling, the total angular momentum without nuclear spin, on the Rb D_2 line was observed with a thin-film absorption cell in a magnetic field on the order of kilogauss [18]. Numerous investigations of the hyperfine Paschen-Back regime in alkali-metal atoms have been performed with a nanocell [19–22]. Baluschev *et al.* observed with a magnetic field strength of a few tens of gauss the region in Rb $5S \rightarrow 5D$ transitions for constructing a laser-lock system [23], and the intensities of the spectra were not of interest to them. Various groups show the importance of understanding the Paschen-Back regime, for example, in multiphoton spectroscopy [24–26], Rydberg states [27], locking the laser frequency for two-photon laser lock [28], and modifying transition strengths at modest magnetic fields for excited states [29].

In this work, we observe the Zeeman and Paschen-Back effects in the $5\,^2S_{1/2} \rightarrow 5\,^2D_{5/2}$ transition of ^{87}Rb with Doppler-free two-photon spectroscopy. By selecting adequate

*abe@phys.chuo-u.ac.jp

polarization, $\sigma^- + \sigma^-$, we confirm the energy shifts and transition rates of these transitions in a weak magnetic field. The Paschen-Back effect is observed in the $5\,^2D_{5/2}$ state in fields as low as several tens of gauss (a few millitesla) while the $5S$ state is still described by the low-field Zeeman effect. Through precise quantitative investigations, we calculate transition rates as a function of magnetic field. While other studies on the Paschen-Back effect are qualitative, in our work, the shifts in the transition frequencies and changes in transition intensities of the $5\,^2S_{1/2} \rightarrow 5\,^2D_{5/2}$ transitions are compared with theoretical calculation results. Quantitative investigation regarding changing the shifts and intensities in the magnetic field leads us to realize applications involving quantitative quantum control of spin states [11,30,31].

II. THEORY

In this section, we describe the effect of a magnetic field on an atom in two-photon spectroscopy. A Hamiltonian without an electromagnetic field (electric dipole transition) is given by

$$\begin{aligned} H &= H_0 + H_B \\ &= H_0 - \frac{\mu_B}{\hbar}\mathbf{B}\cdot(g_J\mathbf{J} + g_I\mathbf{I}), \end{aligned} \tag{1}$$

where H_0 is the Hamiltonian of the atom without an external field, μ_B is the Bohr magneton, $\mathbf{B}$ is the external magnetic field, $\mathbf{J}$ is the total angular momentum including the orbital angular momentum and electron spin momentum, $\mathbf{I}$ is the nuclear spin momentum, and g_J and g_I are the Landé g factors for each momentum $\mathbf{J}$ and $\mathbf{I}$, respectively. H_0 is expressed as [32]

$$\begin{aligned} H_0 &= A_{\rm hfs}\mathbf{I}\cdot\mathbf{J} \\ &\quad + B_{\rm hfs}\frac{3(\mathbf{I}\cdot\mathbf{J})^2 + 3/2(\mathbf{I}\cdot\mathbf{J}) - I(I+1)J(J+1)}{2I(2I-1)J(2J-1)} \end{aligned}$$

and

$$\begin{aligned} &\langle F, m_F|H_0|F, m_F\rangle \\ &= \frac{1}{2}A_{\rm hfs}K + B_{\rm hfs}\frac{(3/2)K(K+1) - 2I(I+1)J(J+1)}{4I(2I-1)J(2J-1)}, \end{aligned}$$

where $A_{\rm hfs}$ is the magnetic dipole hyperfine constant, $B_{\rm hfs}$ is the electric quadrupole hyperfine constant, $|F, m_F\rangle$ is the eigenstate of H_0, and $K = F(F+1) - I(I+1) - J(J+1)$. The nondiagonal matrix elements of H_0 are zero. In a strong field, the interaction Hamiltonian H_B is diagonal for $|J, m_J, I, m_I\rangle$. On the other hand, for an intermediate field, the interaction Hamiltonian, which now contains off-diagonal matrix elements, is numerically diagonalized to obtain eigenvalues and eigenvectors. The interaction Hamiltonian can be translated to

$$\begin{aligned} \tilde{H}'_B &= \langle J, m_J, I, m_I|H_B|J, m_J, I, m_I\rangle \\ &= -\mu_B B_z(g_J m_J + g_I m_I), \end{aligned}$$

where the quantization axis is z. Using the Clebsch-Gordan coefficient, the basis transformation is written as

$$\begin{aligned} \tilde{H}_B &= \langle F', m_{F'}|H_B|F, m_F\rangle \\ &= U^\dagger \tilde{H}'_B U, \end{aligned}$$

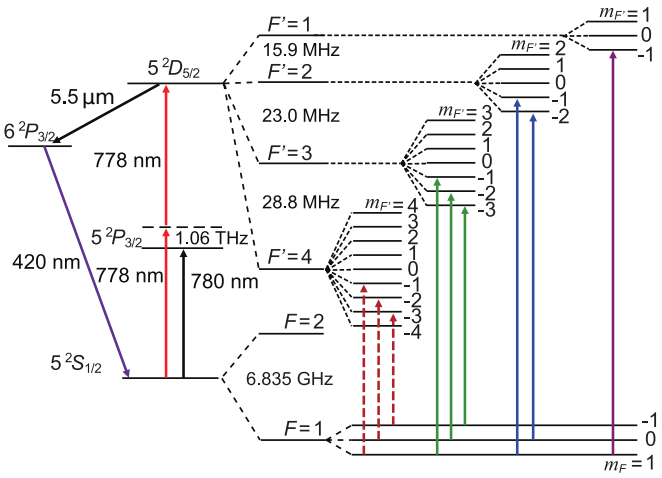

FIG. 1. Energy level diagram of ^{87}Rb. Two-photon excitation occurs via off-resonant levels with 1 THz from the $5\,^2P_{3/2}$ state. In part of the hyperfine level, solid lines indicate allowed transitions ($\Delta F = 0, 1, 2$ and $\Delta m_F = -2$). Dashed lines show additional transitions induced by a magnetic field.

where

$$U = \sum_{m_J, m_I}\langle F, m_F|J, m_J, I, m_I\rangle.$$

Although $\tilde{H}_B$ has nondiagonal matrix elements, the matrix has blocks corresponding to a given m_F. The block corresponding to each value of m_F is diagonalized, and the obtained eigenvectors are written as

$$|\psi(F, m_F)\rangle = \sum_{F^{(i)}} c_{F,F^{(i)}}|F^{(i)}, m_F\rangle. \tag{2}$$

When the energy shift due to the magnetic field is small compared to the hyperfine splittings, F is treated as a good quantum number. For strong fields where the appropriate interaction is described by Eq. (1), the interaction term H_B dominates the hyperfine energies, so that the hyperfine Hamiltonian perturbs the strong-field eigenstates $|J, m_J, I, m_I\rangle$.

Next, we review two-photon spectroscopy [3]. It is possible to eliminate momentum transfer between the electromagnetic field(s) and atom and consequently eliminate Doppler shifts. This characteristic assures that excited D states in alkali-metal atoms can be investigated with high spectroscopic resolution. The momentum transfer relations are written as $\Delta\omega_{\rm D} = (k_L - k_L)v = 0$, where $\Delta\omega_{\rm D}$ is the first-order Doppler broadening, k_L is the beam wave vector, and v is the velocity of the atom. The reason for the minus sign of the second term within the parentheses is that the propagation direction of the second beam is opposite that of the first beam. The Doppler broadening has no effect on this relationship. Therefore, the observed spectra have only a natural linewidth (in reality, this includes the laser linewidth, transit-time broadening, and so on).

Figure 1 shows the energy level diagram of ^{87}Rb. Two-photon excitation occurs via off-resonant levels with 1 THz from $5\,^2P_{3/2}$. The selection rules of two-photon transitions, $\Delta F = 0, \pm1, \pm2$ and $\Delta m_F = 0, \pm1, \pm2$, are satisfied. Our interest is the $\sigma^- + \sigma^-$ configuration with the selection rule

$\Delta m_F = -2$ shown as solid lines in Fig. 1. The Hamiltonian matrix elements of the interaction between an atom and electromagnetic field consist of all hyperfine components corresponding to the ground states and excited states written as

$$\langle \psi(F_e, m_e)|e\mathbf{r}|\psi(F_g, m_g)\rangle = \sum_{F_e^{(i)}, F_g^{(j)}} c_{F_e, F_e^{(i)}} \langle F_e^{(i)}, m_e | e\mathbf{r} | F_g^{(j)}, m_g \rangle c_{F_g, F_g^{(j)}}, \quad (3)$$

where subscripts "g" and "e" denote ground and excited states, respectively. The constants $c_{F_e,F_e^{(i)}}$ and $c_{F_g,F_g^{(j)}}$ are defined in Eq. (2) and $\langle F_e, m_e|e\mathbf{r}|F_g, m_g\rangle$ are the unperturbed transfer coefficients having the following definition:

$$\langle F_e, m_e|e\mathbf{r}|F_g, m_g\rangle = \langle J_e||e\mathbf{r}||J_g\rangle(-1)^{J_g+m_g+I}\sqrt{2J_g+1}\sqrt{2F_g+1} \times \sqrt{2F_e+1}\begin{pmatrix} F_e & 2 & F_g \\ m_e & \Delta m_F & -m_g \end{pmatrix}\begin{Bmatrix} J_g & J_e & 2 \\ F_e & F_g & I \end{Bmatrix}, \quad (4)$$

where ( ) and { } are the Wigner $3j$ and $6j$ symbols, respectively, and $\langle J_e||e\mathbf{r}||J_g\rangle$ is the reduced matrix element of J. The Wigner symbols are second rank owing to the off-resonant two-photon transition. The eigenvalues of the matrix are the probability amplitudes of the $S \rightarrow D$ transition.

III. EXPERIMENTAL APPARATUS

Figure 2 shows our experimental setup for two-photon spectroscopy. A single-frequency titanium sapphire (TiS) laser is employed in this experiment. The power transmitted through the optical isolator is 400 mW, and the linewidth is less than several tens of kilohertz. The main laser beam is divided into two optical paths: one leads to a main cell for magnetic-field-dependence measurements (Main cell, 200 mW) and the other leads to a reference cell (Ref. cell, 200 mW) to which an external magnetic field is not applied. Both beams are polarized as σ^- with quarter-wave plates ($\lambda/4$ plates). The beams are incident on the Rb cells and reflected by mirrors after passing through the cells. The reflected beams counterpropagate along the coaxial paths with a $\sigma^- + \sigma^-$ polarization configuration [33]. Then, Rb atoms are excited to the $5\,^2D_{5/2}$ state via the off-resonant $5\,^2P_{3/2}$ state and emit fluorescence at 420 nm from the transition from $6\,^2P_{3/2}$ to $5\,^2S_{1/2}$ via the $5\,^2D_{5/2} \rightarrow 6\,^2P_{3/2}$ decay (Fig. 1). These fluorescence emissions are detected by photodetectors with optical bandpass filters that allow only 420 nm radiation to pass.

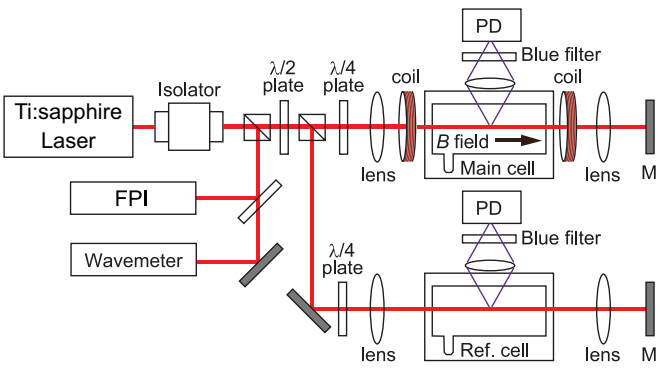

FIG. 2. Experimental setup; two-photon spectra in a magnetic field via $6P \rightarrow 5S$ emission using a photodetector in the main cell can be compared with those without a magnetic field in the reference cell. FPI: Fabry-Pérot interferometer as a frequency marker; M: mirror; $\lambda/4$ plate: quarter-wave plate; $\lambda/2$ plate: half-wave plate.

Parts of the beam from the TiS laser are sent to a Fabry-Pérot interferometer and a wavemeter. The Fabry-Pérot interferometer is used for calibration as a frequency marker. The free spectral range is 752 MHz for 778 nm. As an atom absorbs two photons with frequency ω simultaneously, the marker separation of the Fabry-Pérot interferometer corresponds to 376 MHz in the observed two-photon spectra.

The geomagnetic field and the surrounding magnetic field produced from other instruments are reduced to less than several tens of milligauss with three Helmholtz coils. Additionally, one Helmholtz coil of the main cell generates a homogeneous magnetic field along the incident laser axis in the range from 0 to 45 G. These cells, with a length of 10 cm, are also heated by nichrome wires, and the atom temperature was approximately 90 °C. To reduce the residual magnetic field induced by the current of the nichrome wires, they are made to be bifilar with current flowing in opposite directions. The beam waist and Rayleigh lengths are 40 μm and 5 mm, respectively [34].

IV. RESULTS AND DISCUSSION

Figure 3 shows two-photon excitation spectra in ^{87}Rb $5\,^2S_{1/2}(F = 1) \rightarrow 5\,^2D_{5/2}(F')$ transitions obtained by varying the magnetic field. The origin of the transverse axis is set to the center of the $5\,^2S_{1/2}(F = 1) \rightarrow 5\,^2D_{5/2}(F' = 2)$ transition at 0 G. The magnetic fields in Figs. 3(a), 3(b), 3(c), and 3(d) correspond to 0, 6, 15, and 45 G, respectively. At 0 G the observed spectrum consists of three peaks, which correspond to the $F' = 1$, 2, and 3 components without splitting. In the presence of the magnetic field, the spectra are resolved into m_F components, and these interactions change under large magnetic fields. Each spectrum is fitted to a Voigt function to derive the quantitative contributions of the Lorentzian and Gaussian functions. The observed linewidths are typically 5 MHz (FWHM); the Gaussian and Lorentzian contributions to the width are 4 and 2 MHz, respectively, as determined from the fitting parameters. The Gaussian component consists of transit-time broadening, residual Doppler broadening, and residual Zeeman broadening; the transit-time broadening is estimated to be 2.4 MHz. The Lorentzian component includes the Rabi frequency, natural linewidth, and broadening by an ac Stark shift within the beam profile. The saturation intensity is 0.0132 mW/cm^2, estimated using a natural linewidth of 300 kHz [35]. Figures 3(c) and 3(d) include transitions to $F' = 4$, which are indicated by arrows. These transitions violate the selection rule at zero magnetic field as expressed in $\Delta F = 0, \pm 1, \pm 2$. In the presence of a magnetic field, F ceases to be a good quantum number, and the wave function can be expressed as a superposition of pure and additional states [36]; the

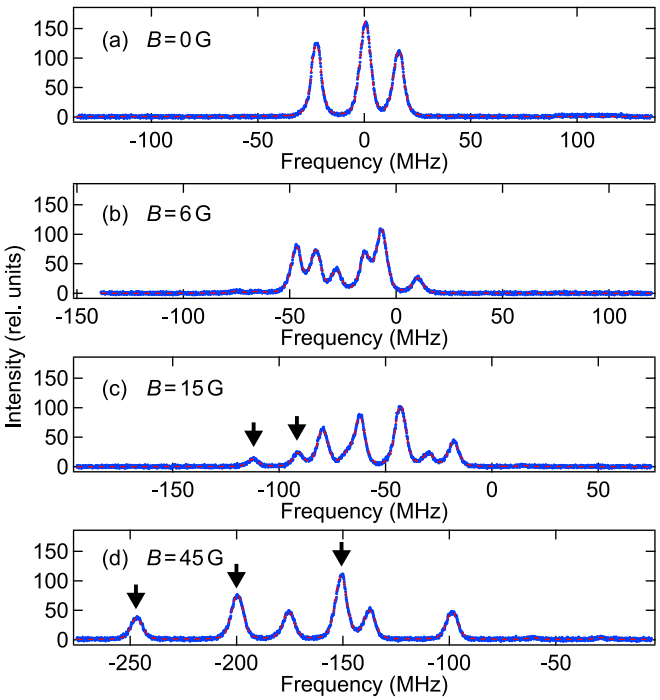

FIG. 3. Observed spectra (blue markers) with fitted ones (red dotted lines) under magnetic fields of (a) 0 G, (b) 6 G, (c) 15 G, and (d) 45 G. Arrows indicate transitions to $F' = 4$. The fits coincide completely with the experimentally measured curve.

$F = 1 \rightarrow F' = 4$ transitions are expressed as dashed lines in Fig. 1.

We acquired the Zeeman spectra in the presence of magnetic fields ranging from 0 G to 45 G in steps of 1 G. The origin of the transverse axis is the same as in Fig. 3. Comparisons between the experimental Zeeman spectra and estimated Zeeman shifts are shown in Fig. 4, where we display the Zeeman spectra at different magnetic field values in steps of 3 G, indicating the excited states $|F', m_{F'}\rangle$. The maximum discrepancy in the fit is 0.5 MHz. Additionally, the error in the magnetic field calibration is estimated to be 2%. The estimated lines are theoretically calculated using the parameters of the S and D states with off-resonant two-photon transitions. These g factors are $g_S = 2.002\ 319\ 304\ 362\ 2$, $g_L = 0.999\ 993\ 69$, $g_I = -0.000\ 995\ 141\ 4$, and $g_{J,S1/2} = 2.002\ 331\ 13$ [32], and the hyperfine constants are $A_{\mathrm{hfs},5S1/2} = 3.417\ 341\ 305\ 452\ 145$ GHz, $A_{\mathrm{hfs},5D5/2} = -7.492\ 3$ MHz, and $B_{\mathrm{hfs},5D5/2} = 1.271\ 3$ MHz [32,35]. We derive $g_{J,D5/2}$ as 1.200 46 from [37]

$$g_{J,D5/2} = g_L \frac{J(J+1) - S(S+1) + L(L+1)}{2J(J+1)} + g_S \frac{J(J+1) + S(S+1) - L(L+1)}{2J(J+1)}. \quad (5)$$

Figure 4 indicates not only the changes in the relative energy shifts but also changes in the relative signal intensities of every line. In particular, the lines identified as $F' = 4$ transitions are observed despite the transition being forbidden in the F basis under a zero magnetic field (assigned $|4, m'_F\rangle$ red lines in Fig. 4). The results show that F ceases to be a good

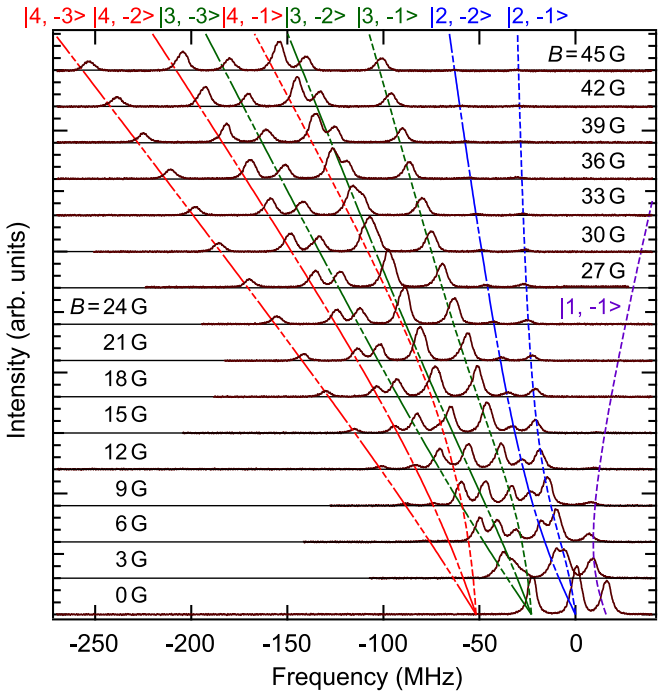

FIG. 4. Zeeman and Paschen-Back effects of transitions $5\,^2S_{1/2}(F = 1) \rightarrow 5\,^2D_{5/2}(F')$; exciting laser light σ^- polarized, $B_{\mathrm{max}} = 45$ G. Each line shows the estimated Zeeman shift and is assigned to each ket vector state. The maximum discrepancy in the fit is 0.5 MHz. Additionally, the error in the magnetic field calibration is estimated to be 2%.

quantum number and a description in the $|J, m_J, I, m_I\rangle$ basis becomes more convenient, otherwise known as the Paschen-Back effect.

We fitted all the acquired spectra and obtained energy shifts and spectrum intensities. Figure 5 shows the dependence of the relative energy shifts between the $5\,^2S_{1/2} \rightarrow 5\,^2D_{5/2}$

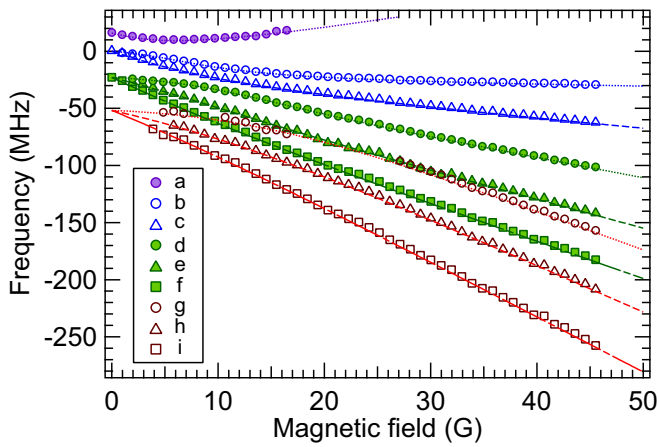

FIG. 5. Relative energy differences between $5\,^2S_{1/2}$ and $5\,^2D_{5/2}$ states in the presence of a magnetic field. Curve (a) corresponds to $F' = 1$, curves (b) and (c) correspond to $F' = 2$, curves (d)–(f) correspond to $F' = 3$, and curves (g)–(i) correspond to $F' = 4$. The markers indicate experimental data, and the dotted lines show calculations of the energy differences. The discrepancy is the same as in Fig. 4.

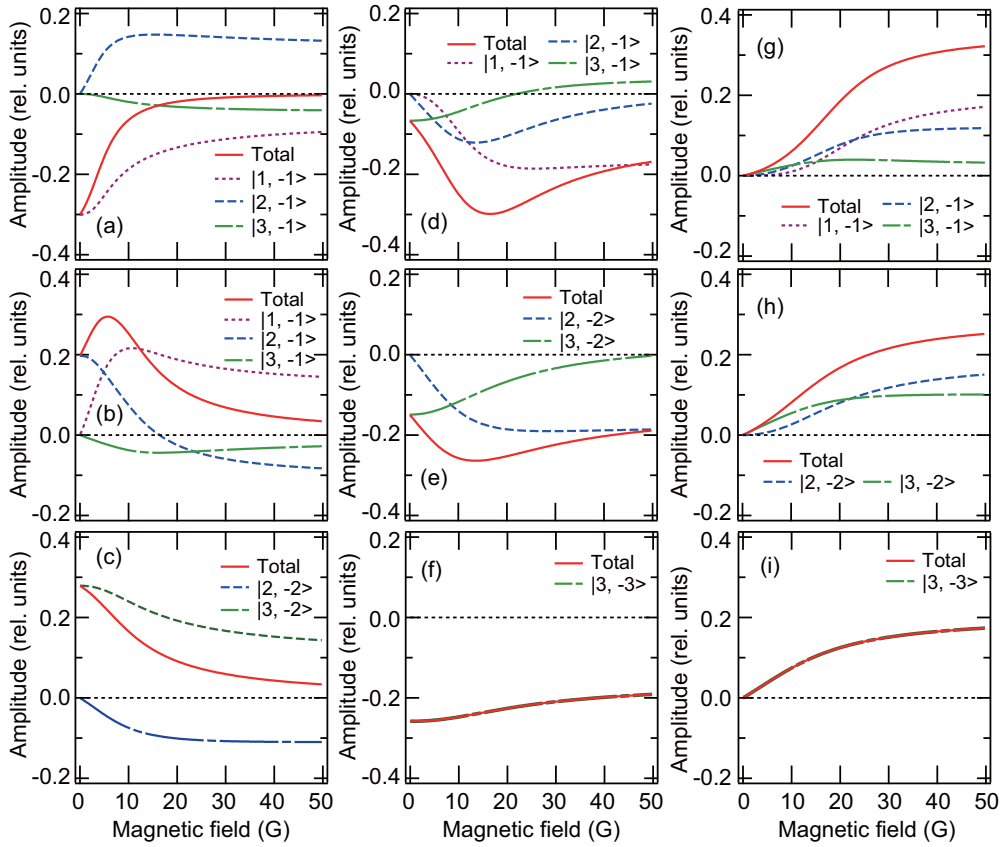

FIG. 6. Dependence of calculation of probability amplitude of $5\,^2S_{1/2} \rightarrow 5\,^2D_{5/2}$ transition on magnetic field with $\sigma^- + \sigma^-$ polarization configuration. The curves (a)–(i) correspond to $|1,-1\rangle$, $|2,-1\rangle$, $|2,-2\rangle$, $|3,-1\rangle$, $|3,-2\rangle$, $|3,-3\rangle$, $|4,-1\rangle$, $|4,-2\rangle$, and $|4,-3\rangle$ in excited states, respectively. Horizontal dotted lines are drawn at zero to guide the eye.

states on the magnetic field for σ^- polarization in two-photon excitation. The discrepancy is the same as in Fig. 4. Despite being in a weak field region of the magnetic field at less than 10 G, we observed energy shifts caused by the Paschen-Back effect. All curves in Fig. 5 approach their corresponding F' states under a zero magnetic field: curve (a) to $F' = 1$, curves (b) and (c) to $F' = 2$, curves (d)–(f) to $F' = 3$, and curves (g)–(i) to $F' = 4$ states. The markers are experimental results. Experimental energy shifts of all F' transitions are in good agreement with those of the calculations. These energy shifts are asymptotic to the m_J basis in a strong field. The results indicate that the wave functions of the D states have their transient and Paschen-Back ranges beyond the LS coupling under a weak magnetic field, whereas those of the S state have this range under a strong field on the order of thousands of gauss [36].

Figure 6 shows the calculated "modified" probability amplitude based on the change in the interaction Hamiltonian H_B depending on the magnetic field; (a)–(i) correspond to $|1,-1\rangle$, $|2,-1\rangle$, $|2,-2\rangle$, $|3,-1\rangle$, $|3,-2\rangle$, $|3,-3\rangle$, $|4,-1\rangle$, $|4,-2\rangle$, and $|4,-3\rangle$ in the excited $5\,^2D_{5/2}$ states, respectively. Each line is derived from a component of Eq. (3). The amplitude of transitions to $|4, m_F\rangle$ at 0 G is 0 [see Figs. 6(g)–6(i)]. The legend "Total" illustrates the normalized transition matrix element $\langle\psi(F', m_{F'})|e\mathbf{r}|\psi(F, m_F)\rangle$ in Eq. (3). All transitions show gradual changes in the transition amplitudes depending on the magnetic field, even in single-component transitions such as those in Figs. 6(f) and 6(i). The components $|4, m_{F'}\rangle$ are zero for any magnetic field strength in all transitions. In view of the "forbidden" transitions to $|4, m_{F'}\rangle$ states, shown in Figs. 6(g)–6(i), the "Total" amplitudes increase with an increasing magnetic field owing to the change in $|3, m_{F'}\rangle$, $|2, m_{F'}\rangle$, and $|1, m_{F'}\rangle$ components, which are "allowed" transitions. We compare the experimental results with the calculated values of the probability intensities as a function of magnetic field by squaring the "Total" in Fig. 6 as shown in Fig. 7. The probability intensities are multiplied by a scaling factor that is determined via least-squares fitting of the measured data, and the same scaling factor is used to multiply all intensity components. The intensities of all the components were fitted using identical fitting parameters. The legends of $|F', m_{F'}\rangle$ illustrate the $5\,^2D_{5/2}$ state. The calculation results are in good agreement with the experimental results for all spin states. At zero magnetic field, F is a good quantum number. Therefore, the intensities of the $|4, m_{F'}\rangle$ transitions are almost zero in weak magnetic fields because the selection rule in the F basis for two-photon transitions, $\Delta F = 0, \pm 1, \pm 2$, is not satisfied. On the other hand, the probability intensities of the $|4, m_{F'}\rangle$ transitions increase with an increase in magnetic field intensities in nonzero magnetic fields, while those of $|1, m_{F'}\rangle$ and $|2, m_{F'}\rangle$ decrease with an increase in the magnetic field intensities. This is explained by the disruption of the hyperfine

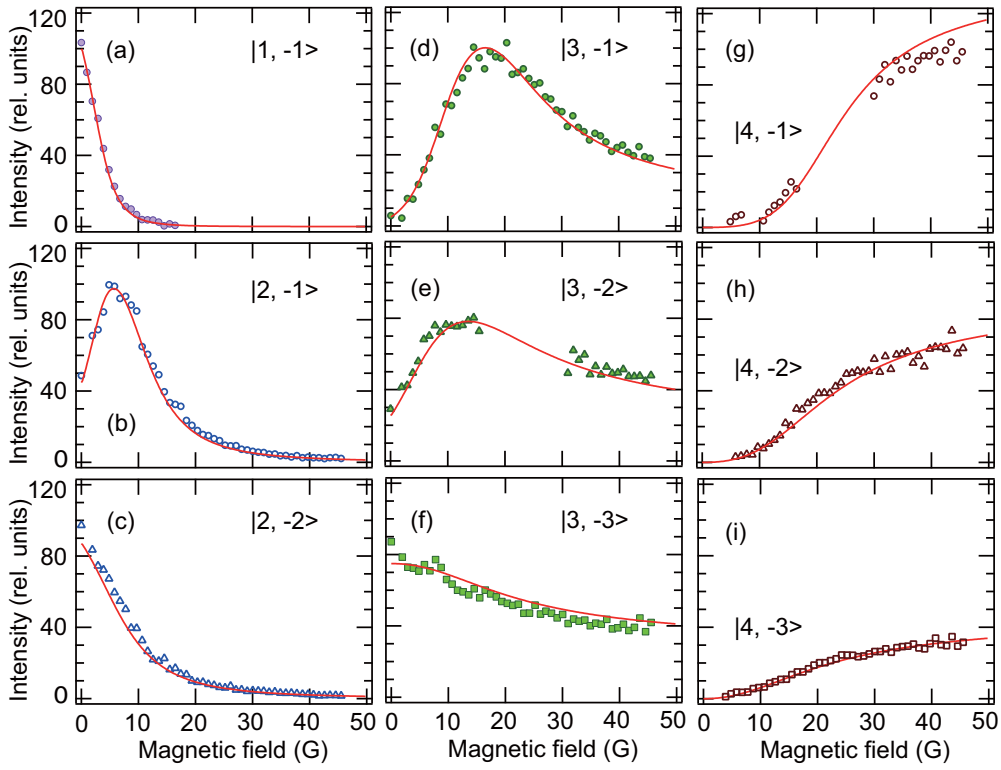

FIG. 7. Plots of observed spectral intensities excited to $|F, m_F\rangle$ in the $5\,^2D_{5/2}$ state. Lines show calculations of the probability intensities as a function of magnetic field by squaring the quantity "Total" in Fig. 6. The probability intensities as a function of magnetic field are multiplied by a scaling factor that is determined by least-squares fitting of the measured data. The intensities for all components were fitted using identical fitting parameters.

coupling of J and I. In Fig. 7, experimental data for the $|3, -2\rangle$ and $|4, -1\rangle$ states are not plotted from 16 to 32 G because spectral lines overlapped and were unresolved in our experiment.

According to the advanced comparisons, some spin states show slight differences between the calculations and experiments. In particular, the calculated values for the $|4, -1\rangle$ state in stronger fields are higher, and those of the $|3, -3\rangle$ state are lower despite the excellent agreement between experiments and calculation in the energy difference, as shown in Fig. 5. Comparison of the intensity behaviors of spin states in the presence of a magnetic field indicates that there may be a change in the g_J factor of the $5\,^2D_{5/2}$ state under stronger magnetic fields condition. For example, using experimental data obtained under magnetic fields below 10 G, we estimated $g_{J,D5/2}(<10\text{ G}) = 1.15$, while we obtained $g_{J,D5/2}$ $(>10\text{ G}) = 1.22$ above 10 G. The detail of the error analysis is described in Appendix A. The difference may be caused by state mixing from about 10 G as shown in Fig. 5 and lead to $g_{J,D5/2}$ being dependent on the magnetic field. In the region over 50 G, where the Paschen-Back effect dominates, $g_{J,D5/2}$ may become independent of magnetic field intensity. The change in the spin state as a function of magnetic field is described in Appendix B.

V. CONCLUSIONS

We observed the Zeeman and Paschen-Back effects in the $5\,^2S_{1/2} \rightarrow 5\,^2D_{5/2}$ transition of ^{87}Rb. The Paschen-Back effect of the $5D$ state occurred under magnetic fields of less than several tens of gauss. Through precise quantitative investigations, we explained the change in the transition rates by varying the magnetic field. Through systematic data collection, energy shifts during the $5\,^2S_{1/2} \rightarrow 5\,^2D_{5/2}$ transitions and transition intensities were compared with results obtained via theoretical calculations. The magnetic field dependence of the $5D$ state will be considerably advantageous to quantum operations in the D state of alkali-metal atoms such as quantum memory [30,31].

ACKNOWLEDGMENTS

We would like to thank K. Shibata for his valuable suggestions. This work was supported by the Matsuo Foundation, the Research Foundation for Opto-Science and Technology, JSPS KAKENHI Grant Nos. JP15K05234 and JP19K03704, and Chuo University Joint Research Grant.

APPENDIX A: ERROR ANALYSIS AS DERIVING g_J FACTOR

Although we fit the data with one scaling factor in Fig. 7, we divide the data into one of $B < B_{\text{bound}}$ and another of $B > B_{\text{bound}}$ and fit each data with an individual scaling factor. Here, B_{bound} is the boundary magnetic field parameter. In each region, we derive g_J factors by assuming that $g_{J,D5/2}$ using all data is 1.20. Figure 8 shows the transient of the square of the standard error of the mean about the data used in Fig. 7

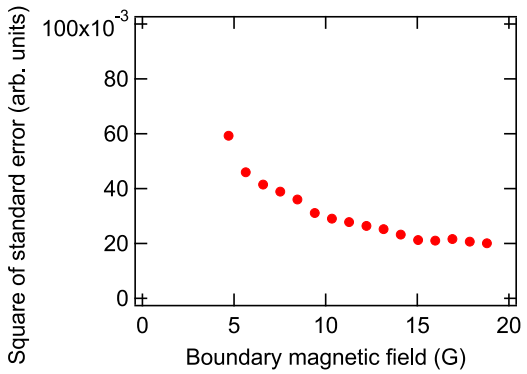

FIG. 8. Transient of the square of the standard error of the mean about the data used in Fig. 7 by varying B_{bound} from 5 G to 20 G as deriving the $g_{J,D5/2}(<B_{\text{bound}})$.

by varying B_{bound} from 5 G to 20 G as deriving the $g_{J,D5/2}$ ($<B_{\text{bound}}$). From $B_{\text{bound}} \sim 10$ G, the square of the standard error of the mean is asymptotic to that using all data.

APPENDIX B: SPIN STATE IN TRANSIENT

The Hamiltonian as shown in Eq. (1) gives the relationship

$$\langle J', m_J', I, m_I | H_0 + H_B | J, m_J, I, m_I \rangle,$$

with the diagonal term for H_B and the nondiagonal term for H_0 due to the operator $\mathbf{I} \cdot \mathbf{J}$. The eigenvectors are obtained when this matrix is diagonalized and grouped by F basis. Figure 9 shows the dependence of the normalized spin coefficients of the $5\,^2S_{1/2} \rightarrow 5\,^2D_{5/2}$ transition on magnetic field intensity in the $|F', m_{F'}\rangle$ basis consisting of $m_{J'}$ components; (a)–(i) correspond to $|1,-1\rangle$, $|2,-1\rangle$, $|2,-2\rangle$, $|3,-1\rangle$, $|3,-2\rangle$, $|3,-3\rangle$, $|4,-1\rangle$, $|4,-2\rangle$, and $|4,-3\rangle$ states for the F basis, respectively. Each $|F', m_{F'}\rangle$ state changes into the corresponding $m_{J'}$ state: $|1,-1\rangle$ into $m_{J'} = +1/2$, $|2,-1\rangle$ and $|2,-2\rangle$ into $m_{J'} = -1/2$, $|3,-1\rangle$, $|3,-2\rangle$, and $|3,-3\rangle$ into $m_{J'} = -3/2$, and $|4,-1\rangle$, $|4,-2\rangle$, and $|4,-3\rangle$ into $m_{J'} = -5/2$. In the m_J basis for the $\sigma^- + \sigma^-$ configuration, the transitions to $m_{J'} = +1/2$ and $-1/2$ in the D state are forbidden owing to spin conservation transitions from $m_J = +1/2$ and $-1/2$ in the S state, whereas the transitions to $m_{J'} = +3/2$ and $+5/2$ are allowed. The results explain why the signal intensities of

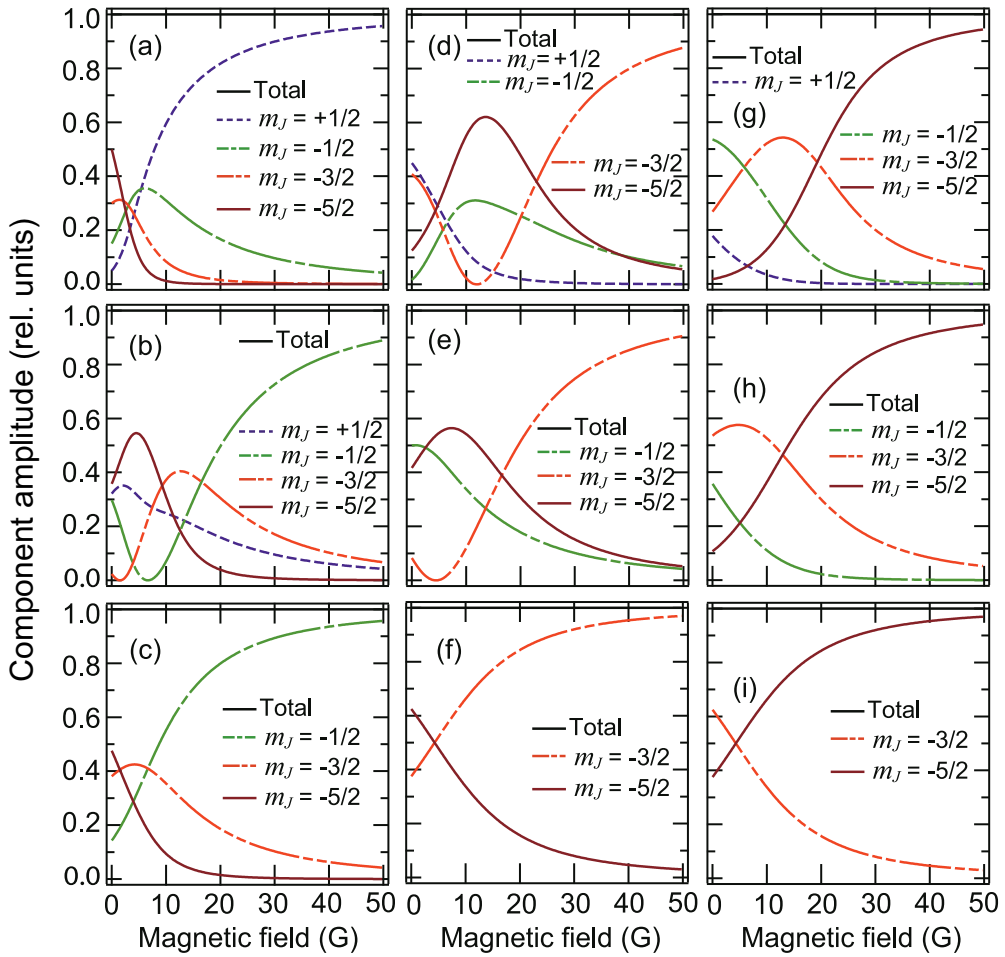

FIG. 9. Dependence of normalized spin constants in $5\,^2S_{1/2} \rightarrow 5\,^2D_{5/2}$ transitions on magnetic field intensity in $|J', m_{J'}\rangle$ basis; (a)–(i) correspond to $|1,-1\rangle$, $|2,-1\rangle$, $|2,-2\rangle$, $|3,-1\rangle$, $|3,-2\rangle$, $|3,-3\rangle$, $|4,-1\rangle$, $|4,-2\rangle$, $|4,-2\rangle$, and $|4,-3\rangle$ states for the F basis, respectively.

the $F' = 1$ and 2 states decrease and those of the $F' = 4$ state increase with an increasing magnetic field. These also indicate that the basis of D states in the presence of a magnetic field becomes the J basis instead of the F basis.

[1] M. M. Salour, Rev. Mod. Phys. **50**, 667 (1978).

[2] J.-W. Pan, Z.-B. Chen, C.-Y. Lu, H. Weinfurter, A. Zeilinger, and M. Zukowski, Rev. Mod. Phys. **84**, 777 (2012).

[3] N. Bloembergen and M. D. Levenson, *Doppler-Free Two-Photon Absorption Spectroscopy* (Springer, Berlin/Heidelberg, 1976), pp. 315–369.

[4] L. Vasilenko, V. Chebotaev, and A. Shishaev, Pis'ma Zh. Eksp. Teor. Fiz. **12**, 161 (1970) [JETP Lett. **12**, 113 (1970)].

[5] B. Cagnac, G. Grynberg, and F. Biraben, J. Phys. France **34**, 845 (1973).

[6] F. Biraben, B. Cagnac, and G. Grynberg, Phys. Rev. Lett. **32**, 643 (1974).

[7] P. Tremblay, A. Michaud, M. Levesque, S. Thériault, M. Breton, J. Beaubien, and N. Cyr, Phys. Rev. A **42**, 2766 (1990).

[8] D. Budker, W. Gawlik, D. F. Kimball, S. M. Rochester, V. V. Yashchuk, and A. Weis, Rev. Mod. Phys. **74**, 1153 (2002).

[9] D. M. Stamper-Kurn and M. Ueda, Rev. Mod. Phys. **85**, 1191 (2013).

[10] Y. Kawaguchi and M. Ueda, Phys. Rep. **520**, 253 (2012), spinor Bose-Einstein condensates.

[11] A. I. Lvovsky, B. C. Sanders, and W. Tittel, Nat. Photonics **3**, 706 (2009).

[12] M. A. Zentile, R. Andrews, L. Weller, S. Knappe, C. S. Adams, and I. G. Hughes, J. Phys. B **47**, 075005 (2014).

[13] F. Biraben, B. Cagnac, and G. Grynberg, Phys. Lett. A **48**, 469 (1974).

[14] L. Windholz, Z. Phys. A **322**, 203 (1985).

[15] L. Windholz and M. Musso, Z. Phys. D **8**, 239 (1988).

[16] T. Hansch, K. Harvey, G. Meisel, and A. Schawlow, Opt. Commun. **11**, 50 (1974).

[17] M. Auzinsh, A. Berzins, R. Ferber, F. Gahbauer, L. Kalvans, A. Mozers, and A. Spiss, Phys. Rev. A **91**, 053418 (2015).

[18] A. Sargsyan, A. Tonoyan, G. Hakhumyan, C. Leroy, Y. Pashayan-Leroy, and D. Sarkisyan, Opt. Commun. **334**, 208 (2015).

[19] A. Sargsyan, G. Hakhumyan, C. Leroy, Y. Pashayan-Leroy, A. Papoyan, D. Sarkisyan, and M. Auzinsh, J. Opt. Soc. Am. B **31**, 1046 (2014).

[20] A. Sargsyan, A. Tonoyan, G. Hakhumyan, C. Leroy, Y. Pashayan-Leroy, and D. Sarkisyan, Europhys. Lett. **110**, 23001 (2015).

[21] A. Sargsyan, E. Klinger, G. Hakhumyan, A. Tonoyan, A. Papoyan, C. Leroy, and D. Sarkisyan, J. Opt. Soc. Am. B **34**, 776 (2017).

[22] A. Sargsyan, A. Papoyan, I. G. Hughes, C. S. Adams, and D. Sarkisyan, Opt. Lett. **42**, 1476 (2017).

[23] S. Baluschev, N. Friedman, L. Khaykovich, D. Carasso, B. Johns, and N. Davidson, Appl. Opt. **39**, 4970 (2000).

[24] D. J. Whiting, E. Bimbard, J. Keaveney, M. A. Zentile, C. S. Adams, and I. G. Hughes, Opt. Lett. **40**, 4289 (2015).

[25] D. J. Whiting, R. S. Mathew, J. Keaveney, C. S. Adams, and I. G. Hughes, J. Mod. Opt. **65**, 713 (2018).

[26] D. J. Whiting, N. Šibalić, J. Keaveney, C. S. Adams, and I. G. Hughes, Phys. Rev. Lett. **118**, 253601 (2017).

[27] L. Ma, D. A. Anderson, and G. Raithel, Phys. Rev. A **95**, 061804(R) (2017).

[28] R. S. Mathew, F. Ponciano-Ojeda, J. Keaveney, D. J. Whiting, and I. G. Hughes, Opt. Lett. **43**, 4204 (2018).

[29] T. D. Barrett, D. Stuart, O. Barter, and A. Kuhn, New J. Phys. **20**, 073030 (2018).

[30] Y. Yoshikawa, K. Nakayama, Y. Torii, and T. Kuga, Phys. Rev. Lett. **99**, 220407 (2007).

[31] Q. Glorieux, J. B. Clark, N. V. Corzo, and P. D. Lett, New J. Phys. **14**, 123024 (2012).

[32] E. Arimondo, M. Inguscio, and P. Violino, Rev. Mod. Phys. **49**, 31 (1977).

[33] A. J. Olson, E. J. Carlson, and S. K. Mayer, Am. J. Phys. **74**, 218 (2006).

[34] A. Yariv and P. Yeh, *Photonics: Optical Electronics in Modern Communications (The Oxford Series in Electrical and Computer Engineering)* (Oxford University Press, New York, 2006).

[35] F. Nez, F. Biraben, R. Felder, and Y. Millerioux, Opt. Commun. **102**, 432 (1993).

[36] D. J. Whiting, J. Keaveney, C. S. Adams, and I. G. Hughes, Phys. Rev. A **93**, 043854 (2016).

[37] H. Bethe and E. Salpeter, *Quantum Mechanics of One- and Two-Electron Atoms* (Springer, Berlin/Heidelberg, 1957).